Characterization of Protein Aggregation via Intrinsic Fluorescence Lifetime

Kristian H. Schlick[a], Candace K. Lange[a,b], Gregory D. Gillispie[b*], Mary J. Cloninger[a*]

[a]*Department of Chemistry and Biochemistry, 103 Chemistry and Biochemistry Building, Montana State University, Bozeman, Montana, 59717* [b] Fluorescence Innovations, Inc., 2155 Analysis Drive, Suite C, Bozeman, Montana 59718

Supporting Information

Contents

General Methods. General reagents were purchased from Acros. Concanavalin A (Con A) was purchased from CalBioChem. Glycodendrimers were prepared as described in reference 6. A Quartz Fluorometer Cell (3/Q/10-GL14-C) was purchased from Starna Cells, Inc.

Instrumentation. Fluorescence data was collected on a Varian Eclipse spectrometer that Fluorescence Innovations, Inc. (FI) modified for fluorescence lifetime measurements. The modifications involved: (1) addition of a tunable UV source (components 1-3, Figure S1) as an alternative to the usual flashlamp excitation source; (2) installation of a R7400 photomultiplier tube (PMT)(component 4, Figure S1) in addition to the standard R928 PMT (component 5, Figure S1), and (3) introduction of a transient digitizer to capture time domain information on the nanosecond time scale. It should be noted that introduction of the laser source and the alternative PMT was accomplished without impacting the standard functionality of the Eclipse. It was also equipped with a TLC 50 cuvette holder (Quantum Northwest, WA) for temperature control and magnetic stirring capabilities. A schematic drawing of the modified Eclipse is shown in Figure S1. The components outlined in blue were not utilized in making fluorescence lifetime measurements.

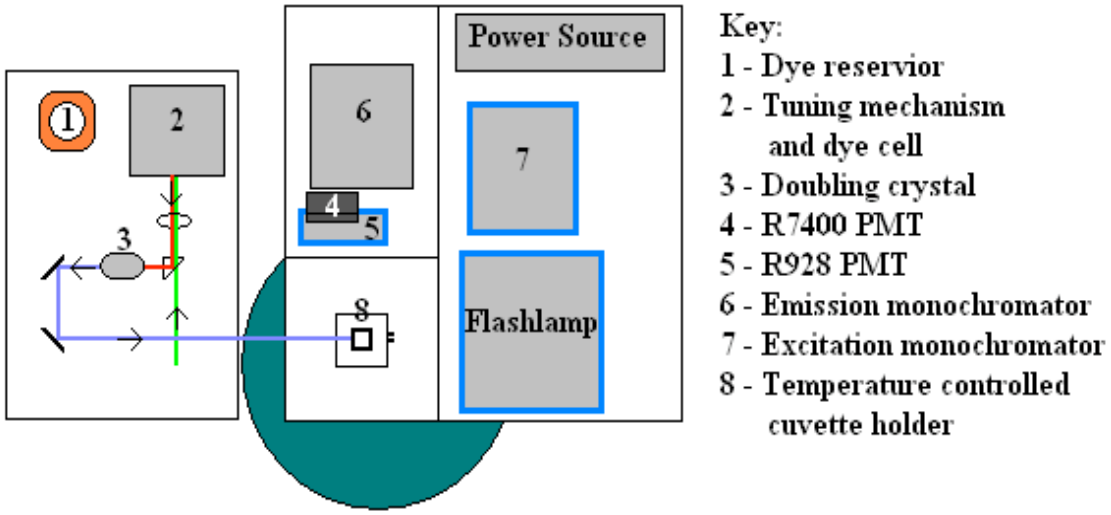

Figure S1. Diagram of Varian Eclipse spectrometer that Fluorescence Innovations, Inc. (FI) modified for fluorescence lifetime measurements. Components are labeled and discussed in the text.

The tunable UV light around 295 nm was generated by pumping a compact dye laser with a pulsed Nd:YAG laser (Teem Photonics, France) and frequency doubling the output. The pump laser is directed into the flow cell, just passing over the right angle prism (Figure S2).

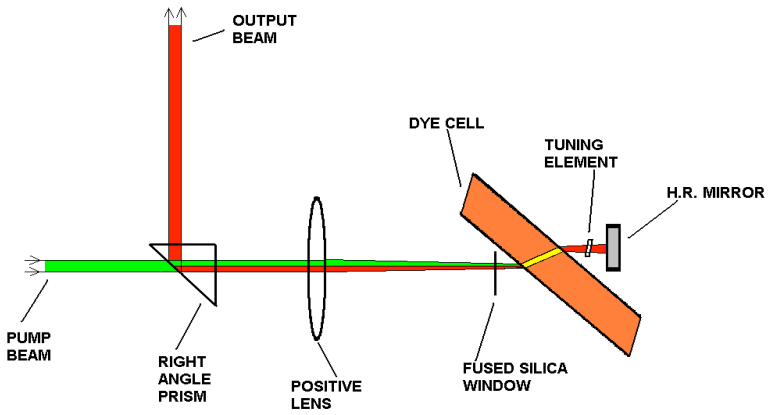

Figure S2. Schematic drawing of dye pumped laser configuration. The dye used was Rhodamine 6G pumped by a Nd:YAG source.

A high reflector (H.R.) mirror reflects the output beam back through the tuning element, which can be rotated to select the excitation wavelength. The doubling crystal converts 560-600 nm light to 280-300 nm. Dichroic mirrors, capable of reflecting UV and passing visible light, remove any reflected green light from the UV beam. The UV laser pulse repetition frequency (PRF) is determined by the 1 kHz Nd:YAG pump source. This is low compared to conventional time domain fluorometers, which operate at MHz frequencies. The high PRFs are not necessary in FI's instrument due to implementation of a transient digitizer and lasers with higher pulse energy. The higher pulse energy increases the number of photons emitted and the transient digitizer collects every photon per pulse, improving the photon statistics.

The sample fluorescence is separated using the emission monochromator equipped in the Eclipse (component 6, Figure S1). In a standard Eclipse, a mirror redirects the wavelength-selected photons emerging from the exit slit to a Hamamatsu R928 PMT. However, this PMT is not suitable for collecting *precise* lifetime data on a nanosecond time scale because the PMT transit time is dependent on where the photocathode is irradiated. Therefore, a Hamamatsu R7400 PMT was installed. To retain functionality of the Eclipse, it was mounted on an adjustable slide. For lifetime measurements it sits at the exit slit of the emission monochromator and can be moved to the side for conventional use of the Eclipse.

The signal from the R7400 PMT is sent to FI's patented transient digitizer. The sampling rate of the digitizer is 1 GHz with 5 times interleaving, or effectively 200 ps time steps. The entire fluorescence decay curve is measured for every laser pulse, rather than laboriously building up the decay curve one photon event at a time, as is the case with time-correlated single photon counting (TCSPC). This method of digitizing measures lifetime data very rapidly, on the order of 100 times faster than conventional TCSPC. Because FI was able to implement lasers with 10,000 times higher energy per pulse, in exchange for lower PRF, one can easily record the contributions of many thousands of photon events per excitation pulse. This results in better photon statistics and higher precision data.

Linear Combination Analysis. By considering the decay spectra as vectors, we are able to utilize all data points rather than condensing them to a single value, as done in iterative reconvolution. Experimentally, we are able to define two vectors describing the fluorescence decay of both free and complexed forms of Con A (blue and pink curve, respectively, Figure S3).

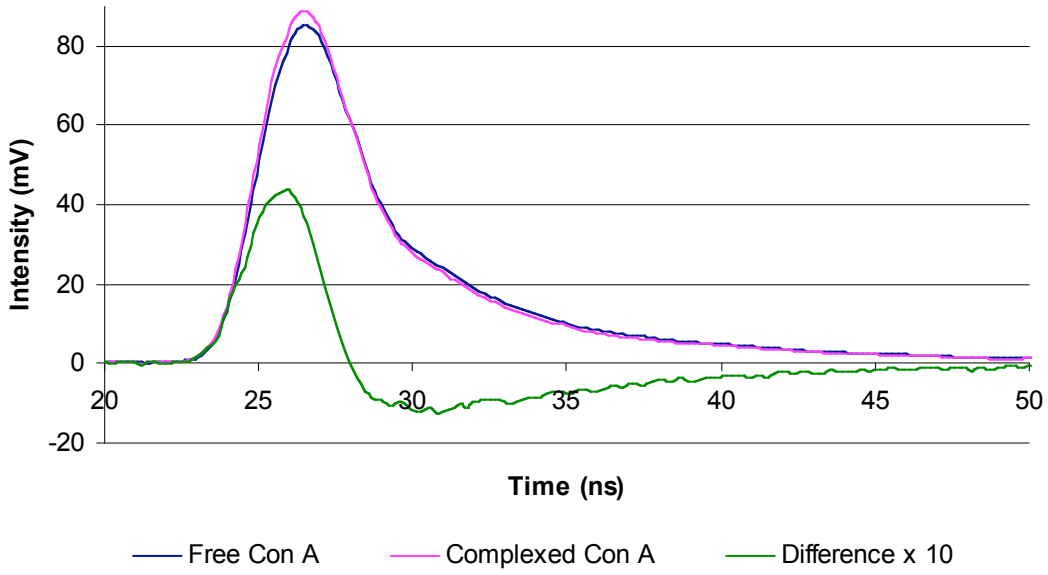

Figure S3. Normalized free and complexed Con A waveforms along with their difference scaled by a factor of 10.

The free vector is obtained from the baseline taken preceding glycodendrimer addition and the complexed vector from the last thirty seconds of the most concentrated glycodendrimer addition. A linear combination of these two vectors could be used to fit each decay curve (equation 1). Therefore, we shall refer to these vectors as basis waveforms.

$$W_i = c_{if} W_f + c_{ic} W_c \qquad (1)$$

A waveform at time i, (W_i) can be represented by mixing the basis waveforms of the free and complexed Con A (W_f and W_c respectively). The relative amount of each basis waveform is determined by the preceding coefficients. Hence, for any given time i, c_{if} and c_{ic} identifies how much of the free and complexed waveform, respectively, is present. Consequently, the coefficients reveal the concentration of each species at a given time. We are assuming that at maximal dendrimer concentration, all Con A has entered into a protein-protein interaction. This is an approximation.

Representative Data. A representative trial of the complex formation upon addition of glycodendrimer is shown in Figures S4-9.

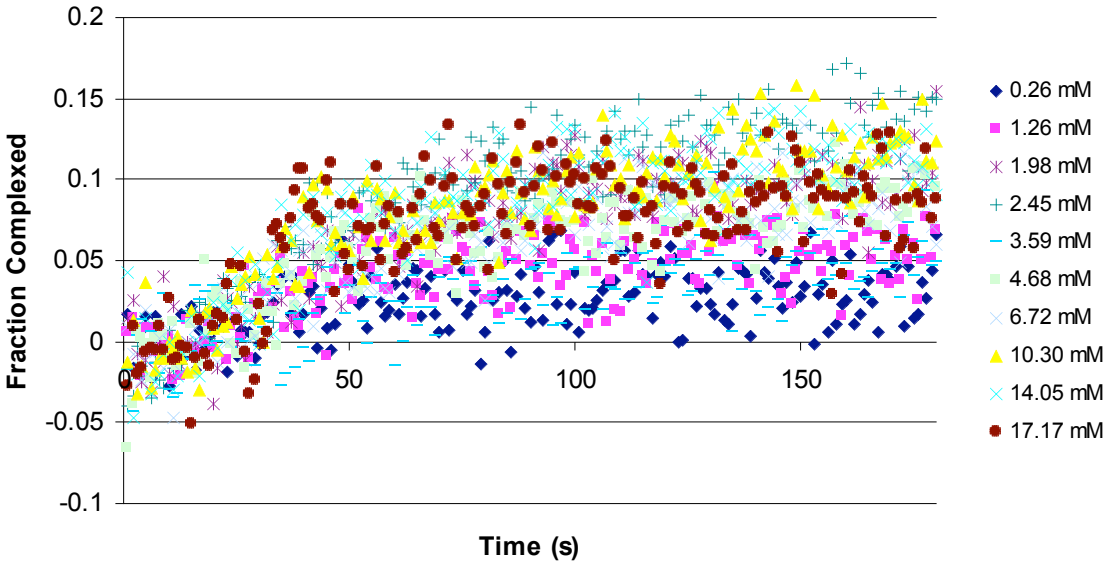

Figure S4. Fluorescence assay data for additions of Me-man into 100 μg/mL Con A.

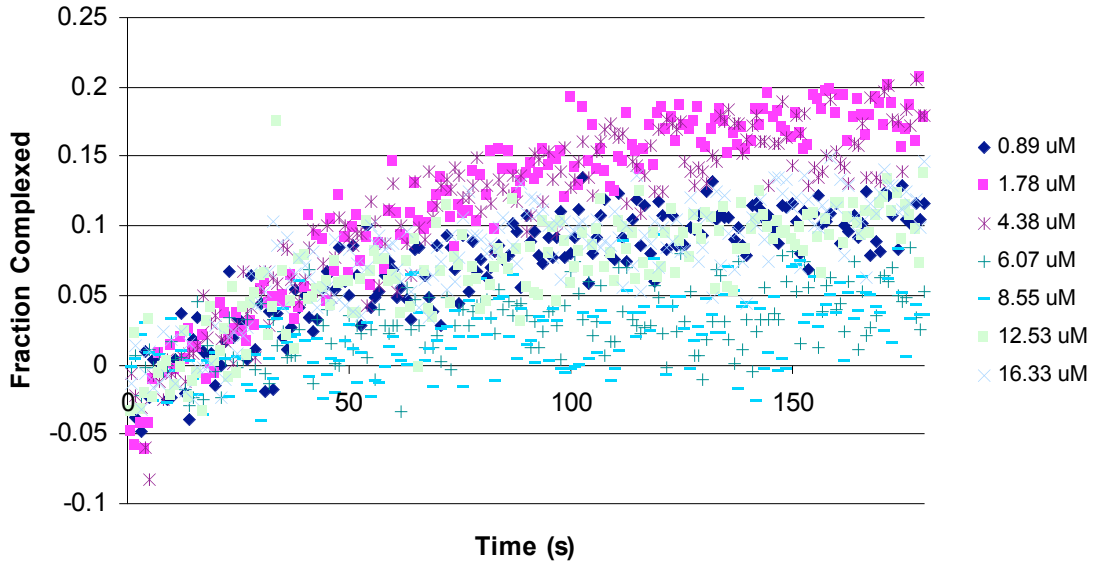

Figure S5. Fluorescence assay data for additions of G(4)-gal into 100 μg/mL Con A.

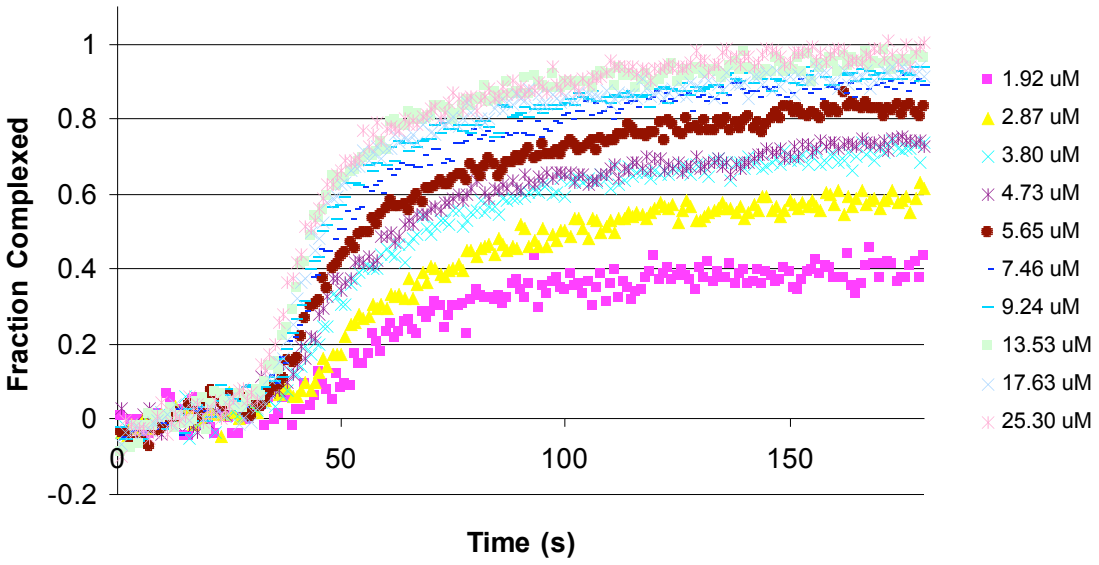

Figure S6. Fluorescence assay data for additions of **1** into 100 μg/mL Con A.

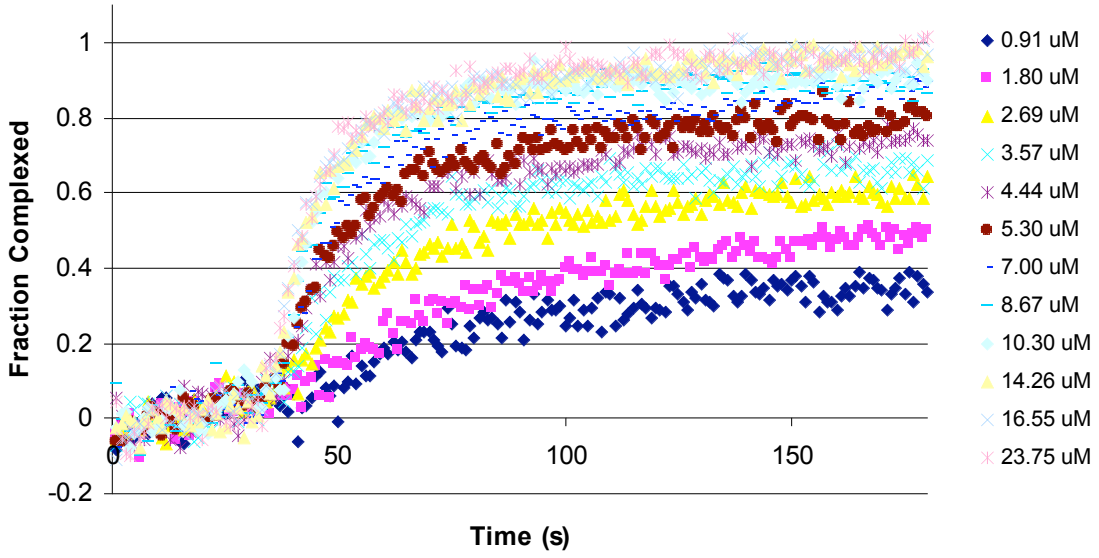

Figure S7. Fluorescence assay data for additions of **2** into 100 μg/mL Con A.

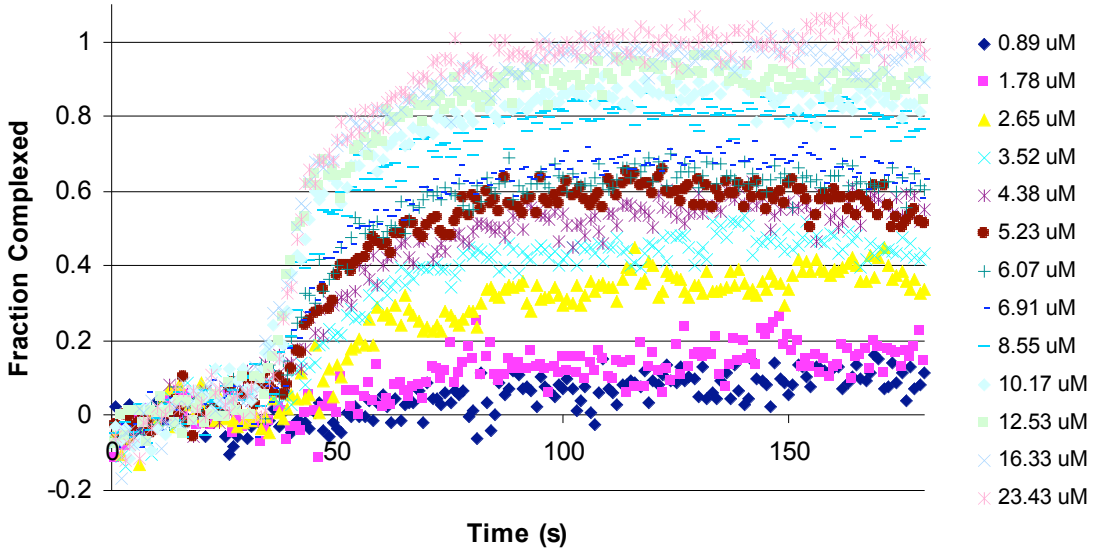

Figure S8. Fluorescence assay data for additions of **3** into 100 μg/mL Con A.

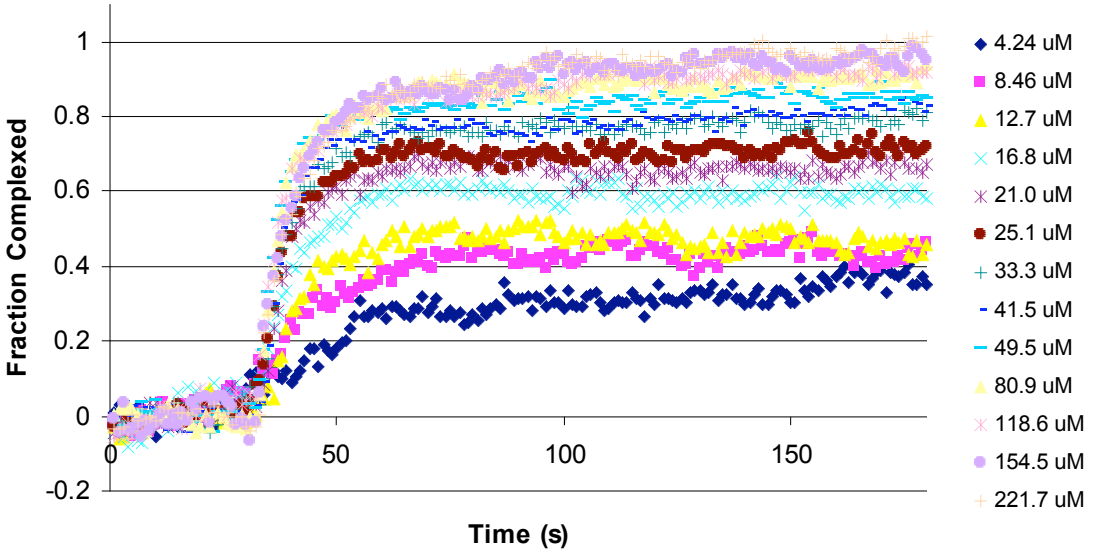

Figure S9. Fluorescence assay data for additions of **4** into 100 μg/mL Con A.

As mentioned in the main text, α *O*-methyl mannoside and G(4) galactose functionalized dendrimer were added to Con-A (Figures S4-S5) to determine the effect of sugar binding as well as non-specific binding of the dendrimer framework to Con-A. Figure S10 emphasizes the minor changes seen for these compounds compared to the corresponding G(4) mannose functionalized dendrimer, suggesting that neither the sugar nor non-specific dendrimer binding causes the fluorescence changes seen.

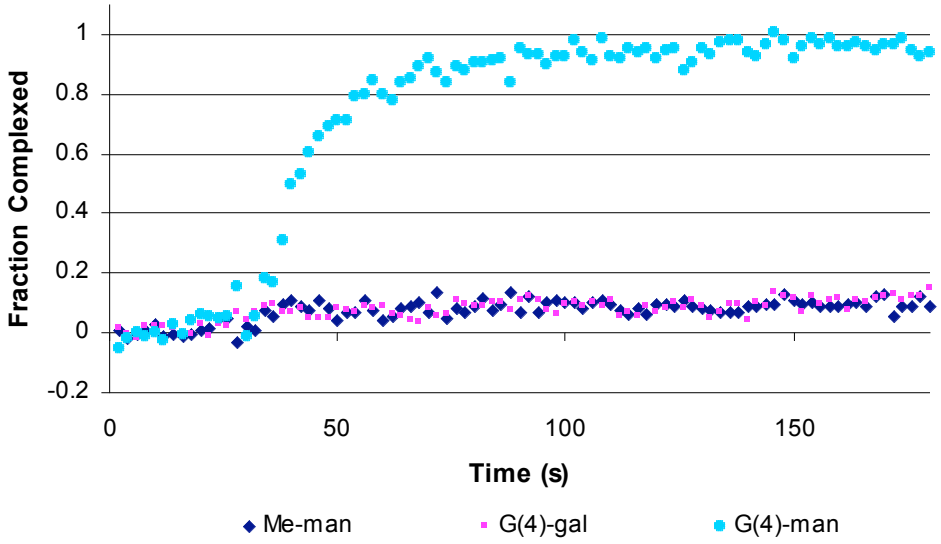

Figure S10. Complex formation upon addition of 17.2 mM Me-man, 16.3 μM G(4)-gal and 16.3 μM G(4)-man **3**.

Complexed Waveform Comparison. The complexed decay curves were compared across glycodendrimer generations and shown to be identical (Figure S11). This supports the statement that all glycodendrimers, regardless of generation, at saturating concentrations formed similar cross-linked states with Con A.

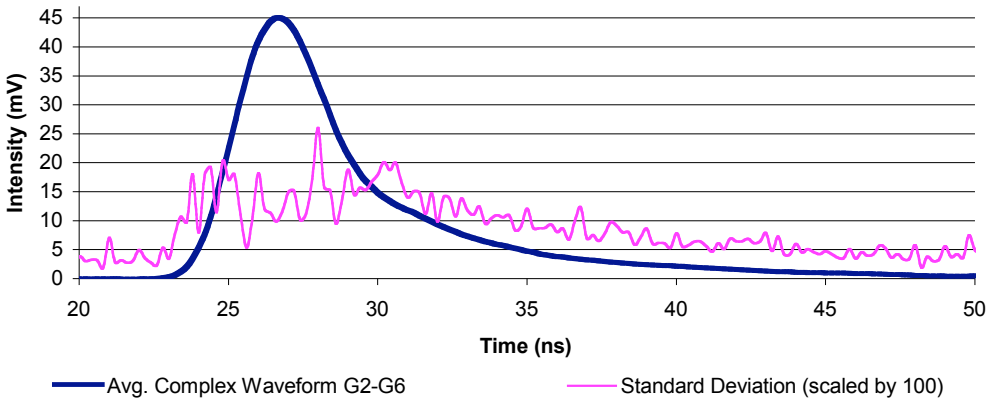

Figure S11. Overlap of complexed waveform for G2-G6 and standard deviation scaled by a factor of 100.

Equilibrium Rate Constant Analysis. The coefficients corresponding to complex formation with time were then used to calculate a k_{obs} for the different glycodendrimer generations using equation 2.

$$\alpha_c(T) = \alpha_{\max}\left(1 - e^{-k_{obs}(T-T_o)}\right) \qquad (2)$$

Where α_{max} is the maximum conversion for a given glycodendrimer concentration, T is time in seconds, T_o is the time of injection, and k_{obs} is the observed binding rate. A non-

linear least-squares fit was used to solve for α_{max}, k_{obs}, and T_o. The bi-phasic nature of the data can be seen in Figure S12. The data was fit to 100 seconds accounting for approximately 90% of the total change. The exceptions were lower generation dendrimer additions, which required all the data be fit. (Figure S13)

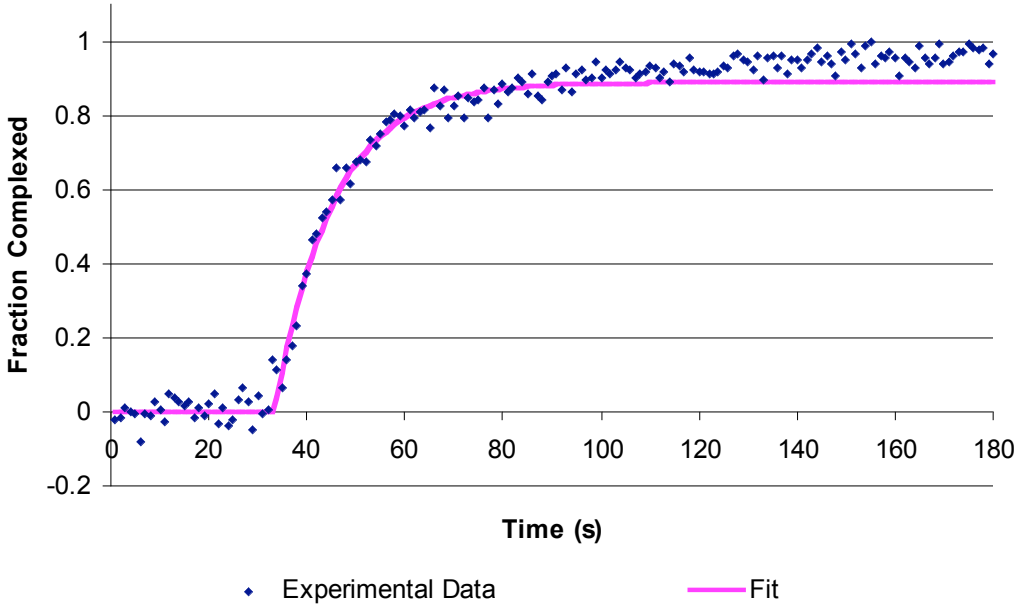

Figure S12. Fit of 14.3 μM G(3)-man data for determination of k_{obs}.

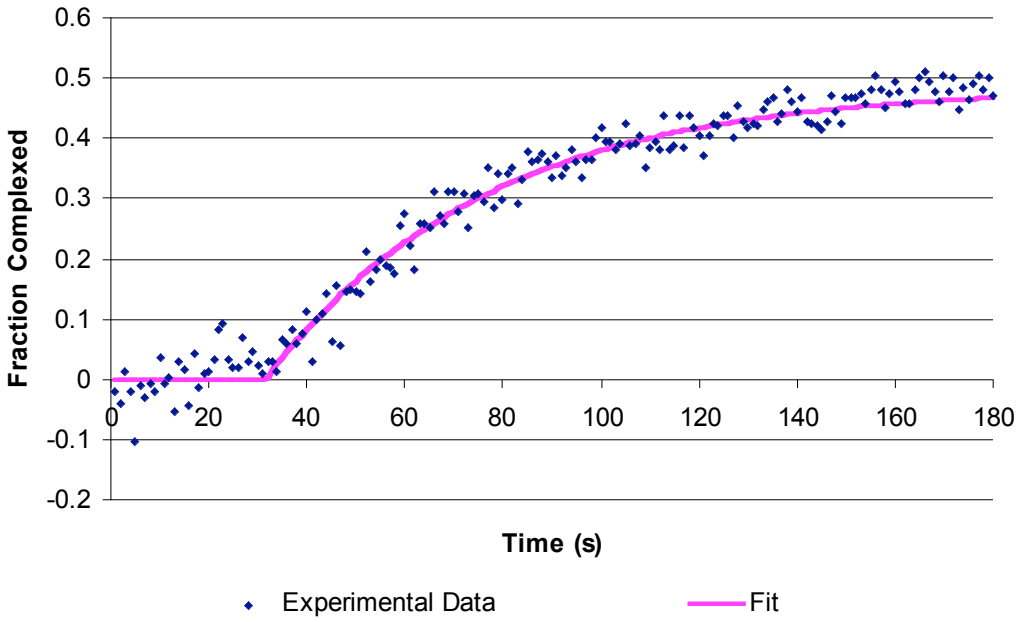

Figure S13. Fit of 1.8 μM G(3)-man data for determination of k_{obs}.

A summary of the calculated k_{obs} values were plotted to emphasize the rate differences for the various glycodendrimer generations at multiple concentrations. (Figures S14 and S15) The values are also shown in tabular form following the graphs. (Tables S1-4) These figures show the increased rate of G(6) compared to the lower generation glycodendrimers, suggestive of multivalent binding.

a)

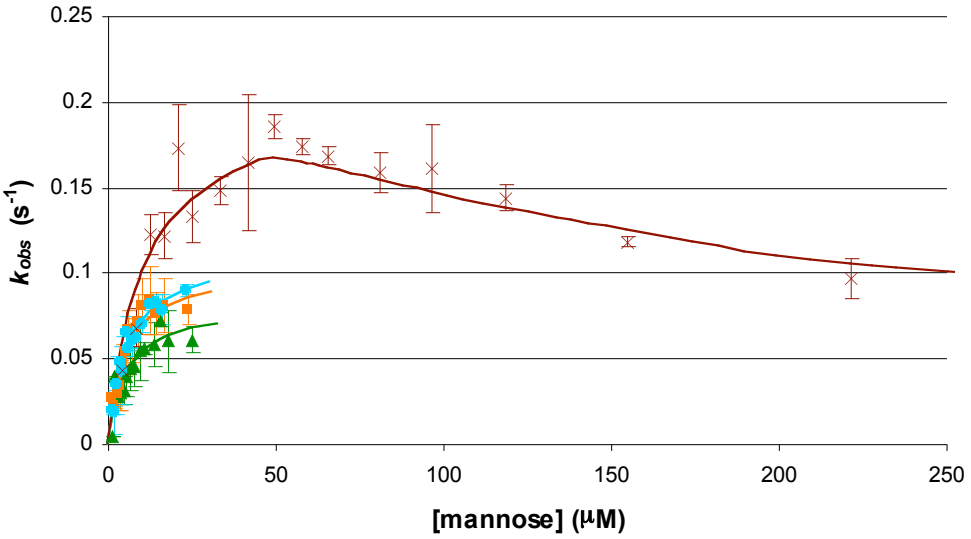

b)

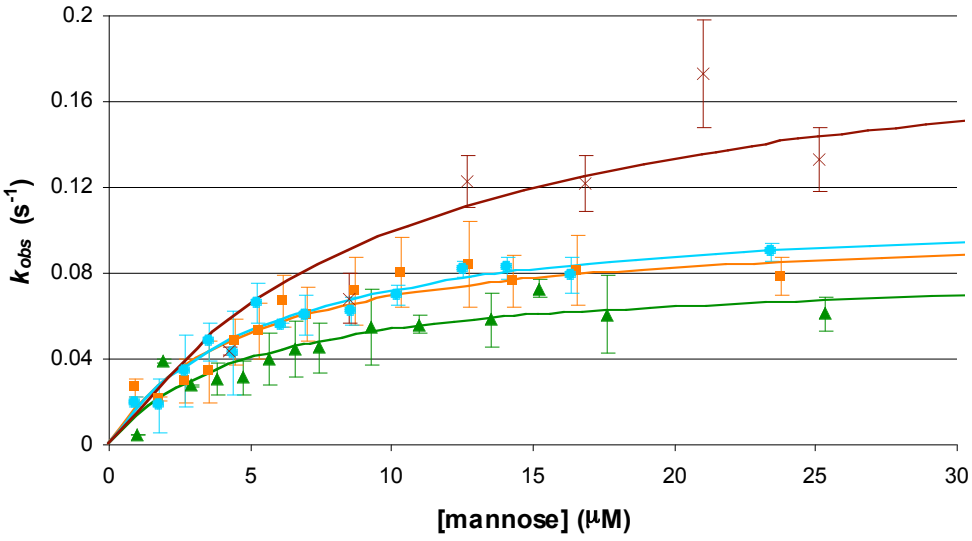

Figure S14. (a) Kinetic data for compounds **1**–**4**. k_{obs} presented on a mannose concentration basis. (b) Expanded view. **1** (▲), **2** (■), **3** (●), **4** (×)

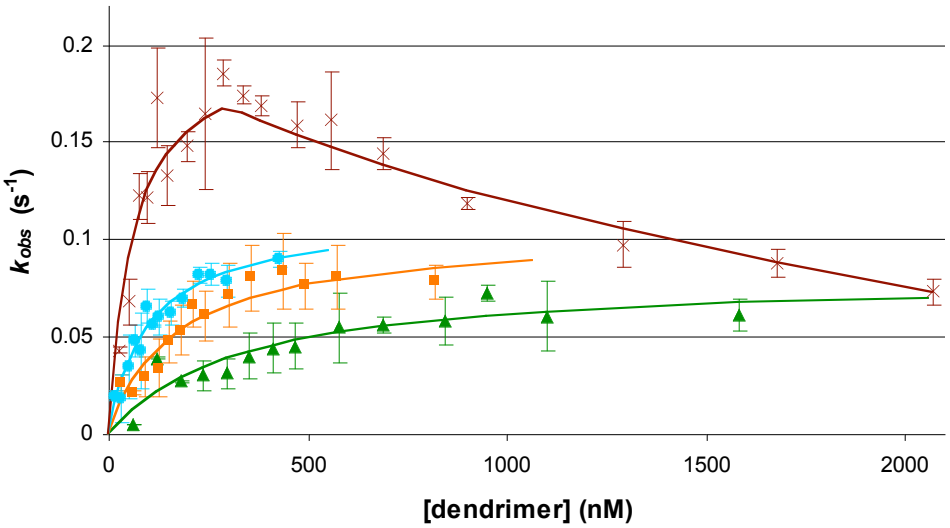

Figure S15. Kinetic Data viewed in terms of dendrimer concentration. **1** (▲), **2** (■), **3** (●), **4** (×)

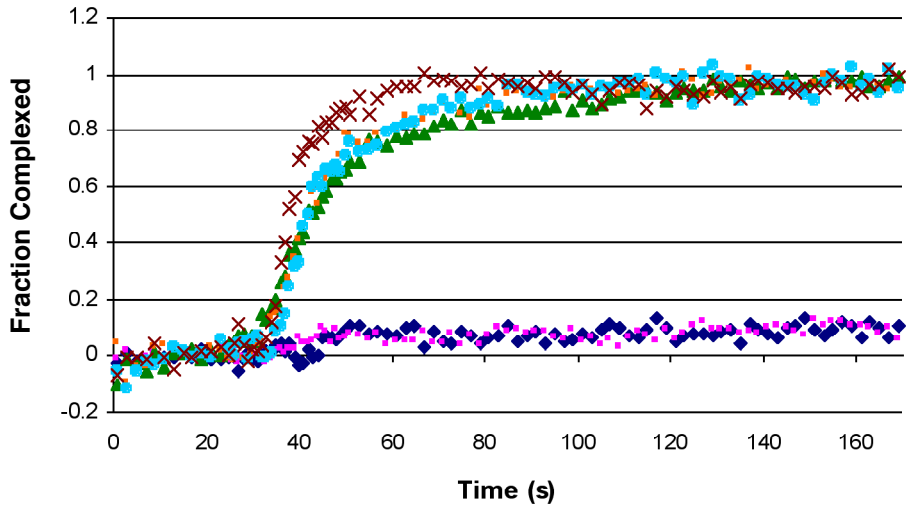

Figure S16. Complex formation of Con A with time as a result of dendrimer addition. 1-O-methyl mannoside (◆, 17.2 mM), galactose-functionalized G(4)-PAMAM (■, 16.3 μM), **1** (▲), **2** (■), **3** (●), **4** (×) (all 21 to 25 μM). Data for mannose-functionalized dendrimers was normalized to the same endpoint to emphasize rate differences between glycodendrimer generations.

Table S1. Calculated k_{obs} for Compound **1**.

G(2)		k_{obs} (sec^{-1})	
[dendrimer] (nM)	[sugar] (μM)	Trial 1	Trial 2
60	0.96	0.0097	0.0022
120	1.92	0.0262	0.0200
179	2.87	0.0203	0.0201
238	3.80	0.0269	0.0200
296	4.73	0.0309	0.0233
353	5.65	0.0295	0.0249
410	6.56	0.0335	0.0262
466	7.46	0.0322	0.0301
577	9.24	0.0389	0.0320
686	11.0	0.0377	0.0336
846	13.5	0.0443	0.0369
950	15.2	0.0418	0.0476
1102	17.6	0.0447	0.0361
1581	25.3	0.0435	0.0366

Table S2. Calculated k_{obs} for Compound **2**.

G(3)		k_{obs} (sec^{-1})	
[dendrimer] (nM)	[sugar] (μM)	Trial 1	Trial 2
31	0.91	0.0136	0.0196
62	1.80	0.0154	0.0200
93	2.69	0.0288	0.0241
123	3.57	0.0365	0.0250
153	4.44	0.0379	0.0288
183	5.30	0.0383	0.0337
212	6.16	0.0460	0.0382
241	7.00	0.0490	0.0367
299	8.67	0.0503	0.0343
355	10.3	0.0528	0.0461
438	12.7	0.0570	0.0419
492	14.3	0.0496	0.0444
571	16.5	0.0543	0.0409
819	23.7	0.0540	0.0442

Table S3. Calculated k_{obs} for Compound **3**.

G(4)		k_{obs} (sec^{-1})	
[dendrimer] (nM)	[sugar] (μM)	Trial 1	Trial 2
16	0.89	0.0131	0.0111
32	1.78	0.0151	0.0167
48	2.65	0.0296	0.0217
64	3.52	0.0345	0.0291
80	4.38	0.0355	0.0380
95	5.23	0.0434	0.0399
110	6.07	0.0443	0.0466
126	6.91	0.0411	0.0451
156	8.55	0.0439	0.0521
185	10.2	0.0484	0.0509
228	12.5	0.0500	0.0561
256	14.1	0.0485	0.0536
297	16.3	0.0503	0.0536
426	23.4	0.0552	0.0558

Table S4. Calculated k_{obs} for Compound **4**.

G(6)		k_{obs} (sec^{-1})	
[dendrimer] (nM)	[sugar] (μM)	Trial 1	Trial 2
25	4.24	0.0440	0.0377
49	8.46	0.0598	0.0633
74	12.65	0.0849	0.0808
98	16.83	0.0956	0.0877
122	20.98	0.1043	0.1258
146	25.12	0.1071	0.0870
194	33.33	0.0914	0.0952
241	41.45	0.1031	0.0842
288	49.50	0.1052	0.0973
334	57.5	0.0898	0.0897
380	65.4	0.0976	0.0921
471	80.9	0.0920	0.0854
559	96.2	0.0915	0.0843
689	119	0.0772	0.0774
898	155	0.0751	0.0684
1289	222	0.0636	0.0558